

Communication

# Cobalt Boride/g-C<sub>3</sub>N<sub>4</sub> Nanosheets-Assisted Electrocatalytic Oxidation of 5-Hydroxymethylfurfural into 2,5-Furandicarboxylic Acid

Mohammed A. Suliman <sup>1</sup>, Chanbasha Basheer <sup>1,2,\*</sup> and Wasif Farooq <sup>3</sup> 

<sup>1</sup> Department of Chemistry, King Fahd University of Petroleum and Minerals, Dhahran 31261, Saudi Arabia; g201403100@kfupm.edu.sa

<sup>2</sup> Interdisciplinary Research Centre for Membranes and Water Security, King Fahd University of Petroleum and Minerals, Dhahran 31261, Saudi Arabia

<sup>3</sup> Department of Chemical Engineering, King Fahd University of Petroleum and Minerals, Dhahran 31261, Saudi Arabia; wasif@kfupm.edu.sa

\* Correspondence: cbasheer@kfupm.edu.sa; Tel.: +966-13860; Fax: +966-13860-4277

**Abstract:** The electrochemical production of 2,5-furandicarboxylic acid (FDCA) from 5-(hydroxymethyl) furfural (HMF) is receiving growing attention. The FDCA-based polyethylene 2,5-furan dicarboxylate (PEF) polymer is a green candidate for substituting polyethylene terephthalate. This work demonstrated a highly efficient CoB/g-C<sub>3</sub>N<sub>4</sub> nanosheet on the surface of the nickel foam as an electrode for the HMF electrooxidation reaction. Electrolysis at a constant potential combined with liquid chromatography showed the formation of FDCA with a yield of 97% with an excellent faradaic efficiency of near 95%. CoB/g-C<sub>3</sub>N<sub>4</sub> achieved a current density of 20 mA cm<sup>-2</sup> for HMF oxidation in 1.0 M KOH with 10 mM HMF at 1.37 V vs. RHE before the competing oxygen evolution reaction. The electrocatalyst was effectively reused up to three times without compromising efficiency. This work demonstrates a cheap and active electrocatalyst material for the electrochemical formation of FDCA from HMF and gives perception into the reaction mechanism.

**Keywords:** 5-hydroxymethylfurfural; electrosynthesis; oxidation; electrocatalyst; FDCA



**Citation:** Suliman, M.A.; Basheer, C.; Farooq, W. Cobalt Boride/g-C<sub>3</sub>N<sub>4</sub> Nanosheets-Assisted Electrocatalytic Oxidation of 5-Hydroxymethylfurfural into 2,5-Furandicarboxylic Acid. *Catalysts* **2021**, *11*, 1241. <https://doi.org/10.3390/catal11101241>

Academic Editors: Lakshmanan Saravanan, Mrinmay Mandal and Shuhui Sun

Received: 1 September 2021  
Accepted: 9 October 2021  
Published: 15 October 2021

**Publisher's Note:** MDPI stays neutral with regard to jurisdictional claims in published maps and institutional affiliations.



**Copyright:** © 2021 by the authors. Licensee MDPI, Basel, Switzerland. This article is an open access article distributed under the terms and conditions of the Creative Commons Attribution (CC BY) license (<https://creativecommons.org/licenses/by/4.0/>).

## 1. Introduction

Recently, value-added product manufacturing from renewable resources has drawn significant interest in the research community [1,2]. The generated 5-hydroxymethylfurfural (HMF) by C6 carbohydrates dehydration has been recognized as one of the top 12 value-added chemicals reported by the United States Department of Energy, obtained from biomass [3]. Through the different catalytic processes, various high-value products and their derivatives have been produced from HMF [4,5]. 2,5-furandicarboxylic acid (FDCA) is a known essential monomer alternative to terephthalic acid.

The transformation of HMF to FDCA can occur in heterogeneous or homogeneous catalysts [6–9]. However, HMF conversion using homogeneous catalysis suffers from poor selectivity and low FDCA yields. Furthermore, it is worth mentioning that using the acidic media reaction would give side reactions that suppress the efficiency of producing FDCA [10].

Electrocatalysis offers an alternative, environmentally friendly route to avoid high pressure and temperature [11,12]. The significant expense of the commonly utilized heterogeneous noble metal catalysts, for example, Ru [13], Pd [14–16], Au [17–20], and Pt [21–25], warrants efforts to succeed them with transition-metal-based catalysts and to discover practical techniques for HMF oxidation. Conventional HMF oxidation to FDCA usually depends on noble metals in high-temperature substances or chemical oxidants and an O<sub>2</sub> pressure reaction [13,25–27]. Electrochemical oxidation in the aqueous medium is an excellent approach. The applied potential drives the response, removing the need for

high pressures of O<sub>2</sub> as an oxidant and the demand for wasteful stoichiometric chemical oxidants. Moreover, the half-reaction of HMF oxidation to FDCA can be combined with value-added products in an electrochemical system, for example, the production of H<sub>2</sub> from water, expanding the general payback and value of the system [10].

High temperatures (80–150 °C) are currently used in the conventional performance for selective HMF oxidation to FDCA utilizing a novel metal base catalyst [28]. One of the challenging tasks is to propose a route for selective HMF oxidation into FDCA under mild conditions.

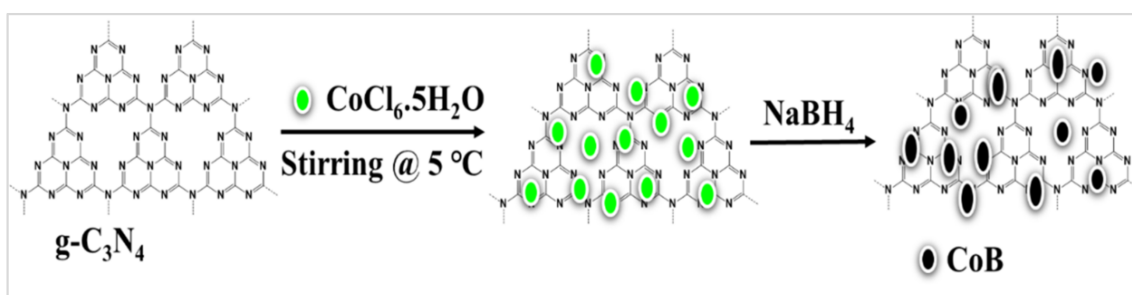
Masa's group described cobalt boride (Ni<sub>3</sub>B) as a prospective electrocatalyst for electrochemical HMF oxidation [29]. In addition, Jonas et al. [30] studied the use of various cobalt metalloid alloys (CoX; X = As, Te, P, Si, B) as potential electrolytes for HMF oxidation, concluding that CoB is the most active electrocatalyst. Furthermore, the use of a Co-based electrocatalyst for HMF oxidation has been investigated [31,32]. Luo et al. [33] presented evidence that the dynamic valence states of Co are determining factors in the selective oxidation of HMF under alkaline conditions. The g-C<sub>3</sub>N<sub>4</sub> is an example of a metal-free photocatalyst that combines the benefits of nontoxicity, high stability, and easy availability [34]. Various methods have been used for g-C<sub>3</sub>N<sub>4</sub> modification, and the best choice is decorated with a co-catalyst. The g-C<sub>3</sub>N<sub>4</sub> bears a π-conjugated system and excellent electron transferability, and high conductivity material.

In this work, g-C<sub>3</sub>N<sub>4</sub> was utilized to support cobalt boride (CoB) to form a hybrid catalyst for selective HMF oxidation to FDCA. Our past work described the effective use of interfacial coupling between the g-C<sub>3</sub>N<sub>4</sub> nanosheet and amorphous CoB nanoparticles as a highly active composite for oxygen evolution reaction (OER) catalyst [35]. To the best of our knowledge, this is the first study of its kind to explore the use of CoB/g-C<sub>3</sub>N<sub>4</sub>@NiF as an electrocatalyst for the electrochemical oxidation of HMF. From this standpoint, we report the electrochemical HMF oxidation into FDCA, which is considered a value-added product catalyzed by nanosheet CoB/g-C<sub>3</sub>N<sub>4</sub> on the nickel foam (NiF) under basic conditions.

## 2. Results and Discussion

### 2.1. Material Characterization

The CoB/g-C<sub>3</sub>N<sub>4</sub> nanosheet synthesis is illustrated in Scheme 1, where g-C<sub>3</sub>N<sub>4</sub> was used as supporting material. The sodium borohydride was used as a reducing agent to form the CoB on the surface of the g-C<sub>3</sub>N<sub>4</sub> nanosheet. TEM confirmed the development of the nanosheet. The morphology (nanoparticles) and size of CoB (~80 nm) are clearly shown in Figure 1c. The scanning electron micrographs (SEM) confirmed the two-dimensional sheets of g-C<sub>3</sub>N<sub>4</sub> SEM of the Cobalt boride catalyst as a particle-like morphology with a uniform dispersion of CoB/g-C<sub>3</sub>N<sub>4</sub> on the surface of nickel foam. The structure of CoB/g-C<sub>3</sub>N<sub>4</sub> was shown in Figure 1a at high magnification. Figure 1b–d shows the bare nickel foam before and after modification by the CoB/g-C<sub>3</sub>N<sub>4</sub> catalyst deposited onto the nickel foam. The preparation of CoB/g-C<sub>3</sub>N<sub>4</sub> on the nickel foam was conducted via the drop-casting method.



Scheme 1. Scheme of synthesis CoB/g-C<sub>3</sub>N<sub>4</sub> composite.

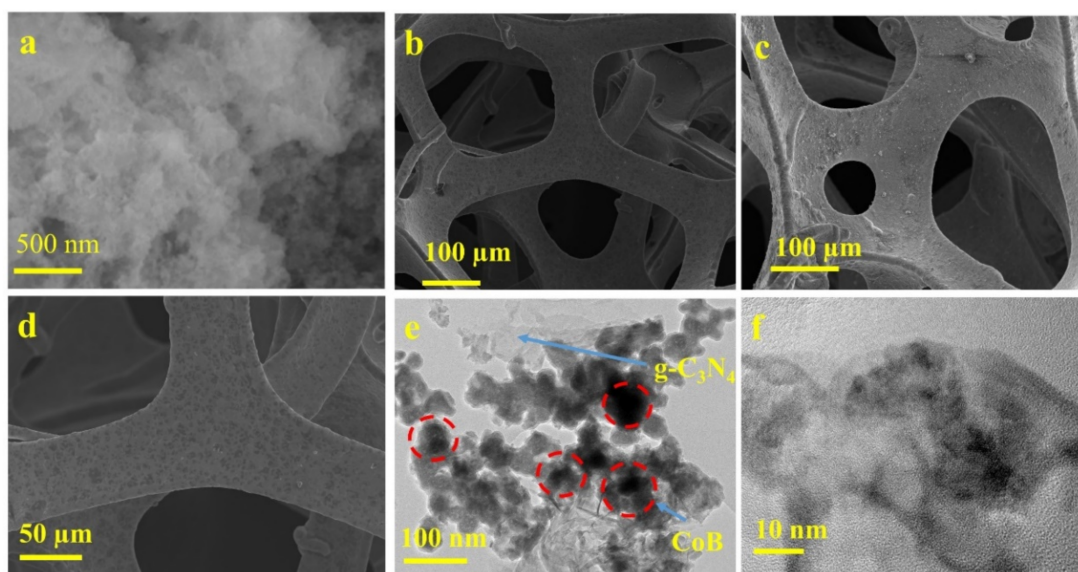


**Figure 1.** (a) SEM of CoB/g-C<sub>3</sub>N<sub>4</sub> high magnification, (b) SEM of bare nickel foam, and (c,d) SEM of CoB/g-C<sub>3</sub>N<sub>4</sub>@NiF, (e,f) TEM of CoB/g-C<sub>3</sub>N<sub>4</sub> at low and high magnification, respectively.

Figure 2a displays SEM elemental mapping images of the as-prepared CoB/g-C<sub>3</sub>N<sub>4</sub>@NiF, showing the complete distribution of the nickel foam by CoB/g-C<sub>3</sub>N<sub>4</sub> catalysts. The mapping proved the existence of nickel, cobalt, carbon, nitrogen, and boron, and their homogenous distribution on the nickel foam's surface (Figure 2b–f). SEM and elemental mapping spectroscopy were used to analyze the structure and composition of the CoB/g-C<sub>3</sub>N<sub>4</sub>@NiF electrocatalyst after the stability test (named post-HMF CoB/g-C<sub>3</sub>N<sub>4</sub>@NiF). The low magnification of Figure S1a,b indicates that the overall structure of the composite has been preserved. However, a thorough examination of the high magnification SEM images (Figure S1c) reveals the presence of featureless monoliths, which are not present in the fresh sample (Figure 1a). The elemental mapping images (Figure S1e) show that the post-HMF CoB/g-C<sub>3</sub>N<sub>4</sub>@NiF consisted of Ni, Co, C, N, B, and an amount of oxygen [36].

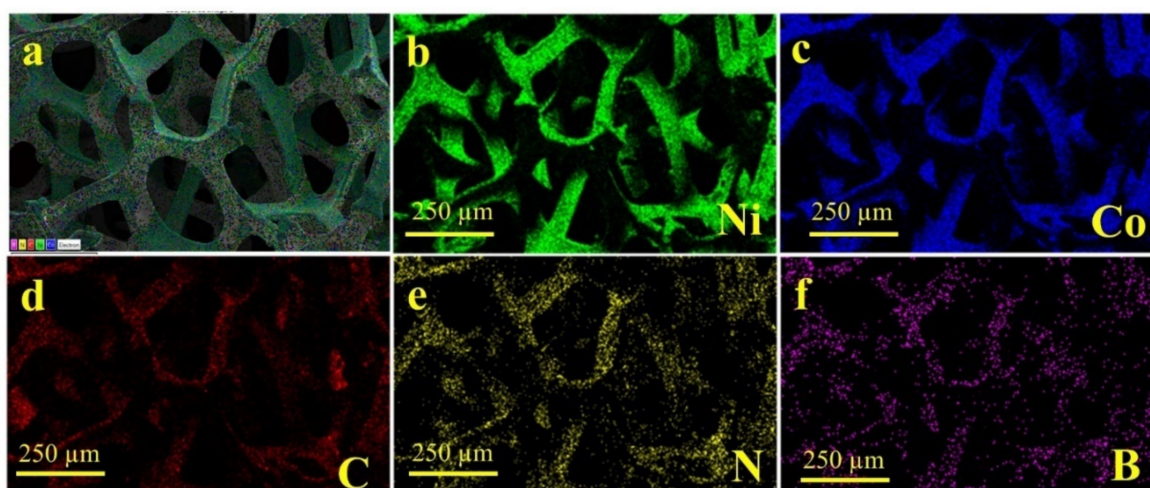


**Figure 2.** Elemental mapping images of the as-prepared CoB/g-C<sub>3</sub>N<sub>4</sub>@NiF; (a) all of the elements are shown together, and the individual ones (b–f) for Ni, Co, C, N, and B shown in the various visible colors.

XPS studied the catalyst surface composition and oxidation states of CoB/g-C<sub>3</sub>N<sub>4</sub>, and the findings are displayed in Table 1. The peak of C 1s at 284.6 eV was retained as a reference to find the elements' binding energy. The core level of the N 1s spectrum can be

divided into three distinct peaks at 399.9, 397.6, and 397.3 eV: The weak peak was caused by the N-(C) 3 groups, and the other peak was caused by the C-N=C bond in which the nitrogen has an  $sp^2$  hybridization. Deconvolution of the C 1s spectrum generated two peaks, centered at 286.73 and 283.66 eV, ascribed to C=N/C=O and C-C, respectively [37]. The high-resolution Co 2p spectrum of CoB/g-C<sub>3</sub>N<sub>4</sub> assigned four peaks at 795.9, 780.7, 802.8, and 785.8 eV, respectively (Table 1).

**Table 1.** XPS table of binding energy for C 1s, N 1s, Co 2p, and B 1s.

Catalyst	Bond Type and Binding Energy (eV)								
	Co 2p (eV)		B 1s (eV)		N 1s (eV)			C 1s (eV)	
CoB/g-C <sub>3</sub> N <sub>4</sub>	Co <sup>2+</sup>	Co <sup>2+</sup>	B-O	Co-B	C-N=C	N-(C) <sub>3</sub>	N-(C) <sub>3</sub> Cyclic	C-C	C=N/C=O
	780.7	785.8	192.0	191.4	397.3	397.6	399.9	283.7	286.7

Two peaks at 795.9 and 802.8 eV were described as two satellite peaks of cobalt (II) ions. The spectra of B 1s of the CoB/g-C<sub>3</sub>N<sub>4</sub> showed a peak at 192.0 eV, related to the boron Oxo-species, and a weak peak at 191.4 eV due to the bear cobalt bond, which confirms the formation of CoB [38]. The spectra of XPS are presented in Figure S2.

CoB/g-C<sub>3</sub>N<sub>4</sub> showed specific surface areas of 86.8 m<sup>2</sup> g<sup>-1</sup>. The surface area was studied using Brunauer–Emmett–Teller (BET) analysis and explored by nitrogen adsorption–desorption isotherms (data not shown). The porous structure of NiF facilitates mass transport, abundant electrolyte contacts interfaces, and increasing active site availability for fast electrochemical kinetic, which improves the electrochemical performance.

## 2.2. Electrochemical Oxidation of HMF

Since it was known that CoB was a very active catalyst for water splitting under strongly basic conditions [39], in this work, we first attempted to study its catalytic performance for HMF oxidation in an alkaline medium. The oxidation of HMF was conducted with a CoB/g-C<sub>3</sub>N<sub>4</sub>@NiF catalyst electrode in a supporting electrolyte composed of 1.0 M KOH. Based on the polarization curve shown in Figure 3, it is clear that linear sweep voltammetry (LSV) of CoB/g-C<sub>3</sub>N<sub>4</sub>@NiF in the absence of HMF shows an anodic current beyond 1.50 V vs. RHE. This catalytic current confirmed the occurrence of the oxygen evolution reaction. The addition of 10 mM of HMF shifts the current catalytic onset to low potential to 1.37 V vs. RHE., which indicates that CoB/g-C<sub>3</sub>N<sub>4</sub>@NiF could preferably catalyze the oxidation of HMF at a lower potential compared to the one required for OER in the basic medium.

The catalytic current density improved dramatically after 1.31 V. It reached a 20 mA/cm<sup>2</sup> current density at 1.37 V vs. RHE, 150 mV less than water oxidation (1.52 V vs. reversible hydrogen electrode (RHE) to arrive at 20 mA cm<sup>-2</sup>). It ought to be noticed that the blank nickel foam (NiF) was less active compared to the HMF oxidation using CoB/g-C<sub>3</sub>N<sub>4</sub>@NiF. Moreover, the previously reported onset potential of 1.25 to 1.3 V vs. RHE is comparable with the Co<sup>4+</sup> formation area observed herein, indicating a similar type of active species [33].

Figure 4a introduces the two-potential pathway for HMF electrochemical oxidation to FDCA. The first path is via the initial oxidation of the aldehyde to yield HMFCa as an intermediate product, while the second path proceeds by the initial oxidation of alcohol to obtain DFF. The latter is unfavorable. The two pathways converge at the formation of FFCA before the final FDCA product [40,41]. To recognize and evaluate the final product and oxidation intermediates of HMF oxidation and decide the Faradaic efficiencies, CoB/g-C<sub>3</sub>N<sub>4</sub>@NiF-catalyzed HMF oxidation was performed at an applied potential of 1.37 V vs. RHE in 10.0 mL of 1.0 M KOH as the supporting electrolyte and with 10 mM of HMF substrate. The transformation of all the HMF to FDCA needs around 58 Coulomb charges if 100% Faradaic efficiency is to be accomplished.

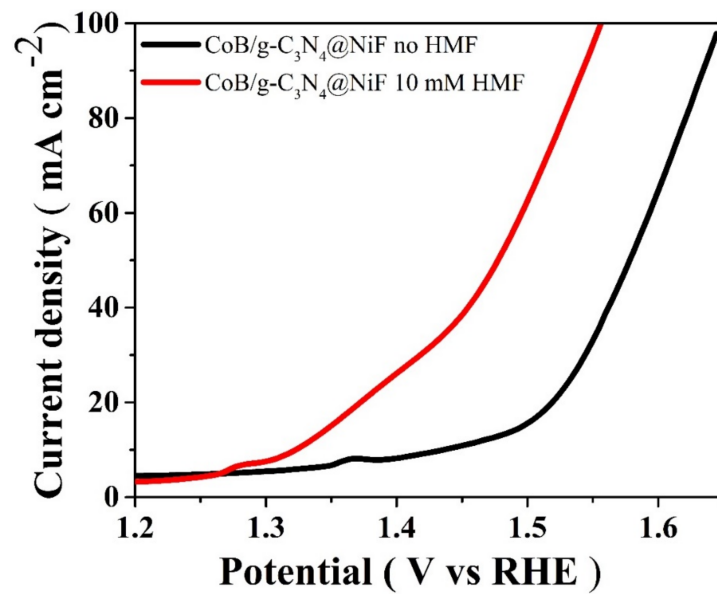


Figure 3. LSV of CoB/g-C<sub>3</sub>N<sub>4</sub>@NiF in the absence and existence of HMF in 10 mM concentration in a supporting electrolyte solution of 1.0 M KOH with a scan rate of 10 mVs<sup>-1</sup>.

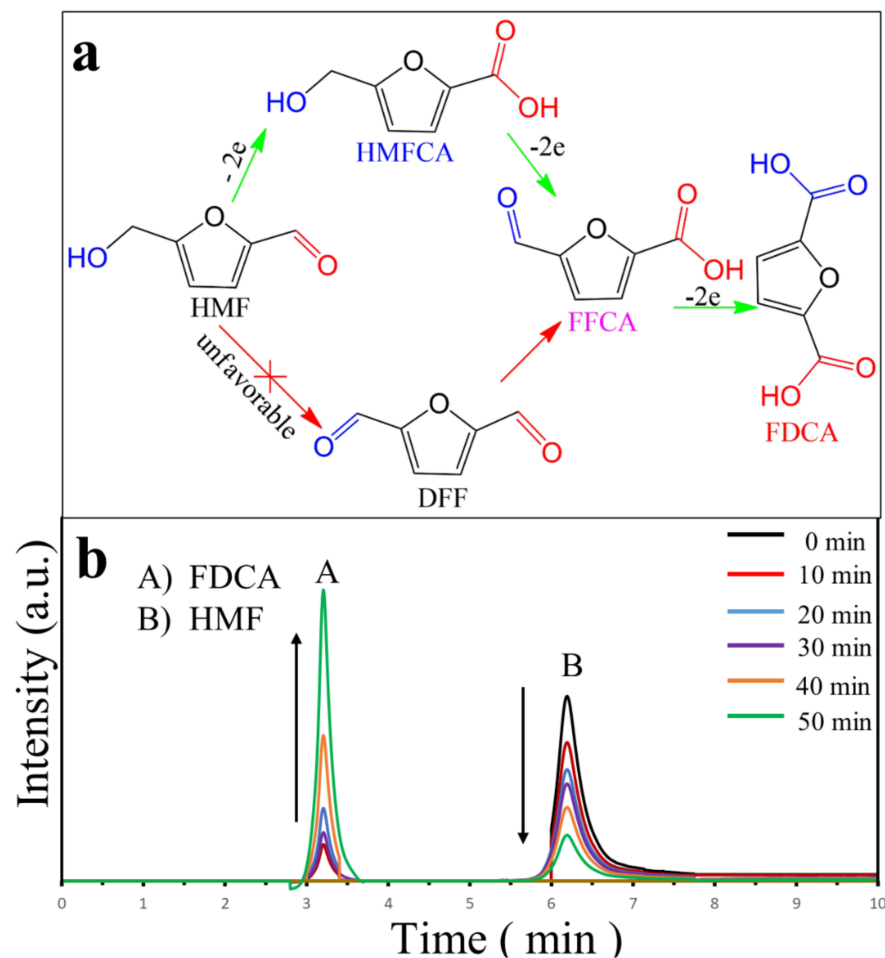
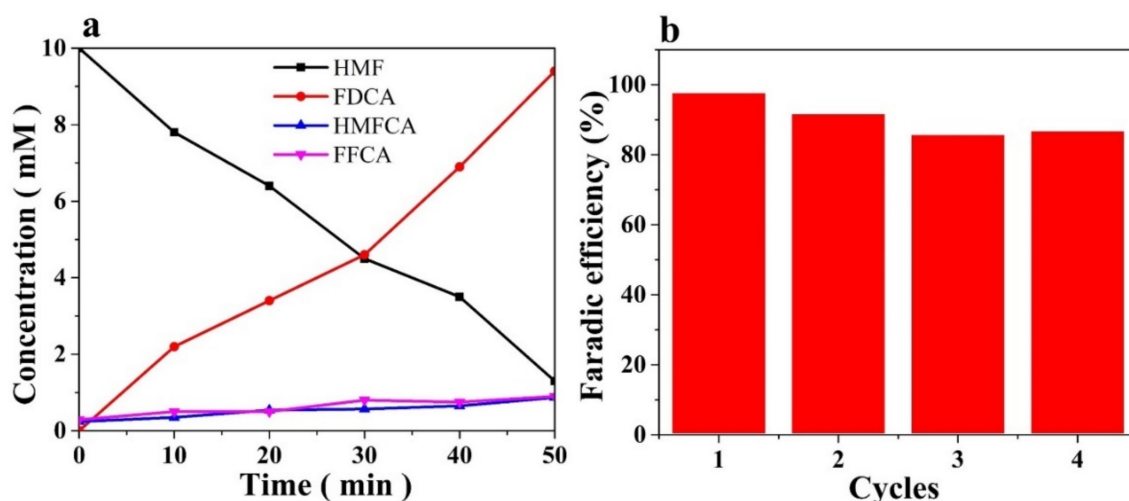


Figure 4. (a) HMF electrochemical oxidation reaction pathways. The first pathway starts with the oxidation of the aldehyde group to form HMFCFA. The second pathway starts with the oxidation of the alcohol group of HMF to give DFF over CoB/g-C<sub>3</sub>N<sub>4</sub>@NiF. (b) HMF concentration change and the oxidation product over electrolysis time.

Liquid chromatography (LC) with a UV detector was used to monitor the reaction after electrocatalysis. Figure 4b shows the oxidation intermediate of HMF (FFCA, 2,5-formylfurancarboxylic acid and HMFCFA, 2,5-hydroxymethylfurancarboxylic acid) and the final oxidation product FDCA during electrolysis. FDCA was the main oxidation product, and the formation of the reaction intermediates was insignificant. It showed the increase in the final formation product and the decline of the HMF over time. The formation of FDCA from HMF is indicated by the decline of HMF and the gradient of FDCA. After passing the charge of approximately 58 Coulomb, the LC trace of HMF vanished even though FDCA increased to the highest value, which indicated the total transformation of HMF.

Figure 5a displayed the HMF change and the yields of possible oxidation intermediate products and eventual outcome during electrolysis. The results show that faradaic efficiencies of 95% for FDCA formation and 93% for HMF conversion are achieved. Electrooxidation of HMF catalyzed by CoB/g-C<sub>3</sub>N<sub>4</sub>@NiF obeyed the steps of aldehyde oxidation through the HMFCFA route (Figure 4a), as shown by the comparatively higher concentration of HMFCFA relative to that of DFF during electrolysis. This route follows that described for aerobic HMF oxidation reactions. However, the DFF route could be omitted, and we noted that the development and utilization of DFF during electrolysis are unfavorable.



**Figure 5.** (a) LC chromatogram traces of the various products at different reaction times following an HMF electrochemical oxidation reaction with the flow rate of 0.2 mL/min. (b) Faradic efficiency CoB/g-C<sub>3</sub>N<sub>4</sub>@NiF with 10 mM HMF in 1.0 M KOH solution for four consecutive electrolyses.

A 64.0% HMF as the starting substrate was transformed into FDCA after 10 min of electrolysis, and residue amounts of FFCA and HMFCFA as intermediates were detected. As the intermediaries do not build up throughout the process, a quick conversion of FFCA and HMFCFA into FDCA is proposed. A complete HMF transformation was accomplished in 50 min along with a high FDCA yield of 96.5%, and 95.0% faradaic efficiency was attained. The remarkably high yield of 98.5% emphasizes the increased activity of CoB/g-C<sub>3</sub>N<sub>4</sub> for electrocatalytic HMF oxidation at the applied potential, particularly considering an HMF decomposition rate of 12%/hour (for a 10 mM of HMF in 1.0 M KOH solution). Transformation of HMF to FDCA is clearly shown in Figure 5a with the decrease in HMF concentration and increase in FDCA concentration over the electrolysis process. The change concentration of HMF and its oxidation intermediates FFCA and FDCA during electrolysis caused unity faradaic efficiency for HMF conversion and the formation of FDCA. Three consecutive cycles were performed to study the robustness toward HMF oxidation, reflecting the robust stability of CoB/g-C<sub>3</sub>N<sub>4</sub>@NiF for HMF oxidation, as shown in Figure 5b.

### 2.3. The Role of CoB/g-C<sub>3</sub>N<sub>4</sub>@NiF for HMF Oxidation

Luo et al. [33] reported an example of selectivity-tuned oxidation of HMF by varying the oxidation states of an electrocatalyst using CoOxHy as the model electrocatalyst. A plausible mechanism is described in which radical species are first produced by the oxidation and deprotonation of the formyl group in HMF. The carbon atom is then further oxidized, and the O atom in H<sub>2</sub>O attacks it to form carboxylate. The CoB/g-C<sub>3</sub>N<sub>4</sub> plays a vital role in the reaction mechanism through a surface phase change and surface structure with a high surface-area-to-volume ratio, making CoB/g-C<sub>3</sub>N<sub>4</sub> an efficient catalyst in basic conditions. It is worth mentioning that the active site in the catalyst was cobalt boride, and the g-C<sub>3</sub>N<sub>4</sub> offered a surface area for both the substrate and the product. Figure 6 illustrates the proposed mechanistic pathway to produce FDCA from HMF. The hydroxide ions attach the carbonyl group to the HMF side by a nucleophilic addition reaction. The formation of geminal diol took place via hydration after a proton departed from the aldehydic group of HMF molecules [29,42,43]. Because of the large hydroxyl groups adsorbed on top of the CoB/g-C<sub>3</sub>N<sub>4</sub>@NiF surface, the dehydrogenation of diol occurs to form the carboxylic group. From that point, the other alcohol part was dehydrogenated due to the deprotonated reaction by the base. The C-H bond activation occurred due to the hydroxide ion and the aldehyde group formation. Electrogenerated Co<sup>3+</sup> and Co<sup>4+</sup> species function as chemical oxidants but play distinct roles in selective HMF oxidation. Luo et al. [33] observed that Co<sup>3+</sup> could only oxidize formyl groups to form carboxylate, but Co<sup>4+</sup> is required for the initial hydroxyl group oxidation with much faster kinetics.

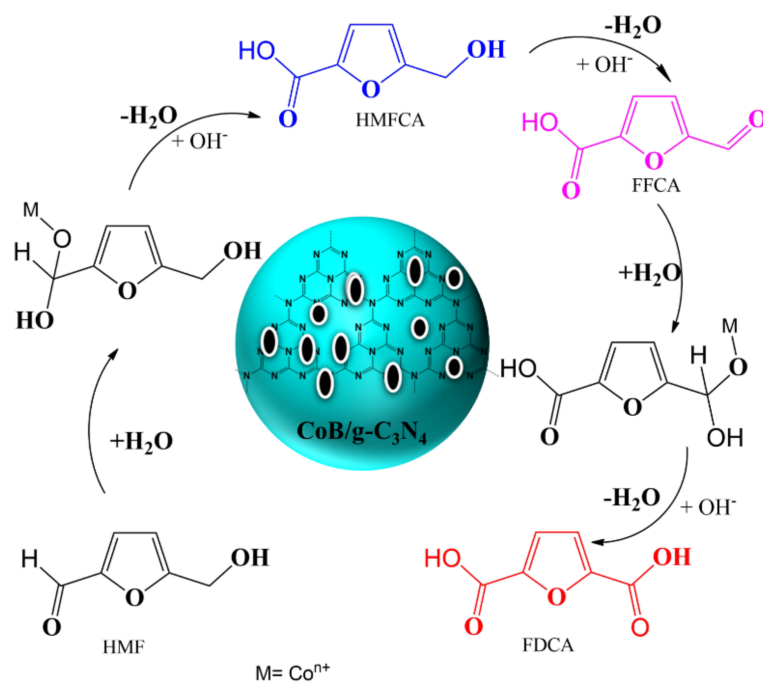


**Figure 6.** Proposed mechanism of the electrochemical HMF oxidation to FDCA over a CoB/g-C<sub>3</sub>N<sub>4</sub> nanosheet.

Table 2 presents a comparison table for our work vs. previously reported literature. Our work revealed that the catalytic activity of CoB/g-C<sub>3</sub>N<sub>4</sub> was significantly higher than previously reported work in the literature.

**Table 2.** Comparison of the total electrolysis performance of dual-function catalysts.

Electrode Materials	Time (hrs)	HMF Conc. (mM)	Electrolyte	HMF Electrooxidation and HER		Faraday Efficiency (%)	FDCA (Yield%)	Ref.
				Current Density (mA cm <sup>-2</sup> )	Potential Window			
CoB/g-C <sub>3</sub> N <sub>4</sub>	~0.8	10	1.0 M KOH	50	1.47	95.0	97.0	This work
				10	1.32	94.3	96.0	
NiCoBDC	1	10	1.0 M KOH	20	1.55	83.1	99.0	[44]
Ni <sub>3</sub> N@C	1	10	1.0 M KOH	50	1.55	99.0	98.0	[45]
				10	1.46			
Ni <sub>2</sub> P	1	10	1.0 M KOH	50	1.58	98.0	98.0	[46]
				10	1.44			
Ni <sub>3</sub> S <sub>2</sub>	1	10	1.0 M KOH	50	1.58	96–99	98.0	[2]
				10	1.46			
Co-P	1	50	1.0 M KOH	20	1.44	100	90.0	[41]
NiCoFe-LDHs	1	5	1.0 M KOH	20	1.51	96.0	~85	[43]
NiOOH	1	5	0.1 M KOH	-	1.47	96.0	96.0	[47]
ACT/TEMPO	4	20	pH 10	-	1.40	93.5	93.5	[48]
CuCo <sub>2</sub> O <sub>4</sub>	1	10	1.0 M KOH	150	1.37	94.0	93.7	[31]
MoO <sub>2</sub> -FeP@C	~2.7	10	1.0 M KOH	-	1.32	97.8	98.6	[49]
N-Ni <sub>3</sub> S <sub>2</sub> -MoO <sub>2</sub>	-	50	1.0 M KOH	20	1.57	90	90	[50]

### 3. Materials and Methods

#### 3.1. Materials

Cobalt chloride ( $\text{CoCl}_2$ ), Sodium borohydride ( $\text{NaBH}_4$ ), Potassium hydroxide (KOH), 5-Hydroxymethylfurfural (HMF), 5-Hydroxymethyl-2-furan-carboxylic acid (HMFCA), 2,5-Diformylfuran (DFF), 2,5-Furandicarboxylic acid (FDCA), and 2-formyl-5-furan carboxylic acid (FFCA), were purchased from Sigma-Aldrich, Dorset, UK. The nickel foam with purity greater than 99.99% was obtained from Sigma-Aldrich. All chemicals were utilized as obtained without any additional purification.

#### 3.2. Synthesis of CoB/g- $\text{C}_3\text{N}_4$ Composite

The synthesis of CoB/g- $\text{C}_3\text{N}_4$  nanosheets was prepared as follows. The as-prepared g- $\text{C}_3\text{N}_4$  was dispersed in a 1:1 ethanol–water mixture solution; the resulting mixture was sonicated for 1 h. After homogenization, an appropriate amount of  $\text{CoCl}_2$  and sodium borohydride were gently added to the solution with stirring at a low temperature. The formation of CoB arises on the surface of g- $\text{C}_3\text{N}_4$ . The method details have been described in our previous work [32].

#### 3.3. Electrode Preparation and Electrochemical Oxidation of HMF

The ink solution was prepared as follows: 5.0 mg of the catalyst, dispersed in 460  $\mu\text{L}$  of water and 500  $\mu\text{L}$  of ethanol, and 40  $\mu\text{L}$  of a 1.66 weight% Nafion solution were added. The resulting mixture was sonicated for at least 1 h to form a homogenous suspension. An appropriate amount of the suspension was deposited on a pre-cleaned nickel foam electrode (1.0  $\text{cm}^2$ ) and allowed to dry under airflow at ambient temperature. The catalyst loading on the NiF electrode was 1.0  $\text{mg cm}^{-2}$ . NiF was selected as a substrate and is stable in basic environments. A three-electrode cell system was used to investigate the activity of the electrocatalyst. The electrochemical oxidation of HMF was measured using a BioLogic VSP-3 potentiostat with a three-electrode configuration. Electrolysis of HMF oxidation experiments was conducted in 30 mL of a 1.0 M KOH solution with 10 mM HMF as substrates. The nickel foam covered with electrocatalysts (1  $\times$  1  $\text{cm}^2$ ) was directly used as the working electrode, while a graphite electrode and an SCE electrode served as the counter electrode and reference electrode, respectively.

#### 3.4. Evaluation of Electrocatalytic Activity

The working electrode CoB/g- $\text{C}_3\text{N}_4$ @NiF, a graphite electrode as a counter electrode, and SCE were employed. The potentials described in this manuscript were converted to the RHE as a reference scale, according to the following equation:

$$E (\text{vs. RHE}) = E (\text{vs. SCE}) + 0.242 \text{ V} + 0.059 \times \text{pH} \quad (1)$$

The electrolyte volume in each electrochemical cell was 25.0 mL. After chronoamperometry measurements, the collection of produced products was taken with a syringe for LC analysis. Before electrochemical tests, high-purity nitrogen was used to bubble the electrolyte solution to eliminate the dissolved oxygen. The electrochemical measurements were conducted utilizing a BioLogic VSP-3 potentiostat electrochemical station at room temperature.

#### 3.5. Product Quantification Using LC

HMF oxidation products were monitored using LC with the following conditions: An electrolyte solution of 10.0  $\mu\text{L}$  was used during chronoamperometry at 1.37 V vs. RHE. A mixture of mobile phase solvents (A and B) was used in LC separation. Solvent A was methanol and solvent B was 5 mM ammonium formate. The quantification and separation were performed by applying an isocratic elution of 30% A and 70% B for a run time of 10 min, at a 0.2  $\text{mL min}^{-1}$  flow rate. The quantification and identification of the product were verified from the calibration curves of commercially purchased pure

reactants, intermediates, and final products. The yield (%) of oxidation products and the conversion (%) of organic substrates were evaluated based on the following two equations:

$$\text{Yield (\%)} = \frac{\text{no. of mole of product formed}}{\text{number of mole of initial substrate}} \times 100\% \quad (2)$$

$$\text{Conversion (\%)} = \frac{\text{no. of mole of substrate consumed}}{\text{no. of mole of the initial substrate}} \times 100\% \quad (3)$$

The product formation faradaic efficiency (FE) was calculated using the following equation:

$$\text{FE \%} = \frac{n \times F \times \text{mole of the product}}{\text{Total charge passed}} \times 100\% \quad (4)$$

$F$  is the Faraday constant (96,485 C/mol) and  $n$  is the electron transfer for each product formation.

### 3.6. Structural Characterizations

The catalyst was characterized by scanning electron microscopy (SEM) with a Thermo-Fisher Energy-dispersive X-ray spectroscopy (EDS) system. The detector at 15 kV and X-ray photoelectron spectroscopy (XPS) was operated on a K-alpha XPS spectrometer (Thermo Scientific ESCALAB 250Xi, Waltham, Massachusetts, USA). Spectra were held in C 1s, N 1s, Co 2p, and B 1s. The binding energy (BE) values were described as the C 1s peak's binding energy of 284.6 eV.

## 4. Conclusions

We have shown the selective and efficient electrocatalytic HMF oxidation into FDCA using cobalt boride dispersed on a graphitic carbon nitride-modified NiF composite in an alkaline medium. A high percentage of FDCA was accomplished at about 95% faradaic efficiency. The intermediates and products formed were examined by LC, showing that oxidation of HMF proceeds through the HMFCA intermediate rather than the DFF pathway. CoB/g-C<sub>3</sub>N<sub>4</sub>@NiF is a promising catalyst for selective electrochemical oxidation of HMF, paving the way toward a green chemistry approach.

**Supplementary Materials:** The following are available online at <https://www.mdpi.com/article/10.3390/catal11101241/s1>, Figure S1: (a–c) SEM picture of post-HMF CoB/g-C<sub>3</sub>N<sub>4</sub>@NiF at various magnifications. (d,e) SEM and the elemental mapping pictures of post-HMF CoB/g-C<sub>3</sub>N<sub>4</sub>@NiF show a uniform distribution of Ni, Co, C, N, and B, as well as a substantial amount of oxygen. Figure S2: XPS spectra of C 1s, Co 2p, B 1s, and N 1s.

**Author Contributions:** Conducted experiment, M.A.S.; designed the experiment and supervised C.B.; analysis, W.F.; investigated the kinetics and reaction mechanism. All authors equally participated in writing the manuscript. All authors have read and agreed to the published version of the manuscript.

**Funding:** The authors acknowledge the funding support of the deanship of scientific research to support this work. DSR-DF181012.

**Data Availability Statement:** Data available are included in the manuscript and the additional data can be accessed from Supplementary Materials.

**Acknowledgments:** Authors would like to acknowledge the support of the Chemistry department, King Fahd University of Petroleum and Minerals (KFUPM), in carrying out this work.

**Conflicts of Interest:** The authors declare no conflict of interest.

## References

1. Michèle, B.; Pierre, G.; Catherine, P. Conversion of Biomass into Chemicals over Metal Catalysts. *Chem. Rev.* **2013**, *114*, 1827–1870.
2. You, B.; Liu, X.; Jiang, N.; Sun, Y. A General Strategy for Decoupled Hydrogen Production from Water Splitting by Integrating Oxidative Biomass Valorization. *J. Am. Chem. Soc.* **2016**, *138*, 13639–13646. [[CrossRef](#)] [[PubMed](#)]

3. Zhou, P.; Zhang, Z. One-Pot Catalytic Conversion of Carbohydrates into Furfural and 5-Hydroxymethylfurfural. *Catal. Sci. Technol.* **2016**, *6*, 3694–3712. [\[CrossRef\]](#)
4. Binder, J.B.; Raines, R.T. Simple Chemical Transformation of Lignocellulosic Biomass into Furans for Fuels and Chemicals. *J. Am. Chem. Soc.* **2009**, *131*, 1979–1985. [\[CrossRef\]](#)
5. Teixeira, I.F.; Lo, B.T.W.; Kostetsky, P.; Stamatakis, M.; Ye, L.; Tang, C.C.; Mpourmpakis, G.; Tsang, S.C.E. From Biomass-Derived Furans to Aromatics with Ethanol over Zeolite. *Angew. Chemie Int. Ed.* **2016**, *55*, 13061–13066. [\[CrossRef\]](#)
6. Latsuzbaia, R.; Bisselink, R.; Anastasopol, A.; van der Meer, H.; van Heck, R.; Yagüe, M.S.; Zijlstra, M.; Roelands, M.; Crockatt, M.; Goetheer, E.; et al. Continuous Electrochemical Oxidation of Biomass Derived 5-(Hydroxymethyl)Furfural into 2,5-Furandicarboxylic Acid. *J. Appl. Electrochem.* **2018**, *48*, 611–626. [\[CrossRef\]](#)
7. Cha, H.G.; Choi, K.S. Combined Biomass Valorization and Hydrogen Production in a Photoelectrochemical Cell. *Nat. Chem.* **2015**, *7*, 328–333. [\[CrossRef\]](#)
8. Hansen, T.S.; Sádaba, I.; García-Suárez, E.J.; Riisager, A. Cu Catalyzed Oxidation of 5-Hydroxymethylfurfural to 2,5-Diformylfuran and 2,5-Furandicarboxylic Acid under Benign Reaction Conditions. *Appl. Catal. A Gen.* **2013**, *456*, 44–50. [\[CrossRef\]](#)
9. Saha, B.; Dutta, S.; Abu-Omar, M.M. Aerobic Oxidation of 5-Hydroxymethylfurfural with Homogeneous and Nanoparticulate Catalysts. *Catal. Sci. Technol.* **2012**, *2*, 79–81. [\[CrossRef\]](#)
10. Kubota, S.R.; Choi, K.S. Electrochemical Oxidation of 5-Hydroxymethylfurfural to 2,5-Furandicarboxylic Acid (FDCA) in Acidic Media Enabling Spontaneous FDCA Separation. *ChemSusChem* **2018**, *11*, 2138–2145. [\[CrossRef\]](#)
11. Zhang, P.; Sheng, X.; Chen, X.; Fang, Z.; Jiang, J.; Wang, M.; Li, F.; Fan, L.; Ren, Y.; Zhang, B.; et al. Paired Electrocatalytic Oxygenation and Hydrogenation of Organic Substrates with Water as the Oxygen and Hydrogen Source. *Angew. Chemie Int. Ed.* **2019**, *58*, 9155–9159. [\[CrossRef\]](#)
12. Jing, Y.; Guo, Y.; Xia, Q.; Liu, X.; Wang, Y. Catalytic Production of Value-Added Chemicals and Liquid Fuels from Lignocellulosic Biomass. *Chem* **2019**, *5*, 2520–2546. [\[CrossRef\]](#)
13. Zhang, Z.; Deng, K. Recent Advances in the Catalytic Synthesis of 2,5-Furandicarboxylic Acid and Its Derivatives. *ACS Catal.* **2015**, *5*, 6529–6544. [\[CrossRef\]](#)
14. Liu, B.; Ren, Y.; Zhang, Z. Aerobic Oxidation of 5-Hydroxymethylfurfural into 2,5-Furandicarboxylic Acid in Water under Mild Conditions. *Green Chem.* **2015**, *17*, 1610–1617. [\[CrossRef\]](#)
15. Mei, N.; Liu, B.; Zheng, J.; Lv, K.; Tang, D.; Zhang, Z. A Novel Magnetic Palladium Catalyst for the Mild Aerobic Oxidation of 5-Hydroxymethylfurfural into 2,5-Furandicarboxylic Acid in Water. *Catal. Sci. Technol.* **2015**, *5*, 3194–3202. [\[CrossRef\]](#)
16. Zhang, Z.; Zhen, J.; Liu, B.; Lv, K.; Deng, K. Selective Aerobic Oxidation of the Biomass-Derived Precursor 5-Hydroxymethylfurfural to 2,5-Furandicarboxylic Acid under Mild Conditions over a Magnetic Palladium Nanocatalyst. *Green Chem.* **2015**, *17*, 1308–1317. [\[CrossRef\]](#)
17. Gupta, N.K.; Nishimura, S.; Takagaki, A.; Ebitani, K. Hydrotalcite-Supported Gold-Nanoparticle-Catalyzed Highly Efficient Base-Free Aqueous Oxidation of 5-Hydroxymethylfurfural into 2,5-Furandicarboxylic Acid under Atmospheric Oxygen Pressure. *Green Chem.* **2011**, *13*, 824–827. [\[CrossRef\]](#)
18. Villa, A.; Schiavoni, M.; Campisi, S.; Veith, G.M.; Prati, L. Pd-Modified Au on Carbon as an Effective and Durable Catalyst for the Direct Oxidation of HMF to 2,5-Furandicarboxylic Acid. *ChemSusChem* **2013**, *6*, 609–612. [\[CrossRef\]](#)
19. Cai, J.; Ma, H.; Zhang, J.; Song, Q.; Du, Z.; Huang, Y.; Xu, J. Gold Nanoclusters Confined in a Supercage of Y Zeolite for Aerobic Oxidation of HMF under Mild Conditions. *Chem. A Eur. J.* **2013**, *19*, 14215–14223. [\[CrossRef\]](#)
20. Miao, Z.; Zhang, Y.; Pan, X.; Wu, T.; Zhang, B.; Li, J.; Yi, T.; Zhang, Z.; Yang, X. Superior Catalytic Performance of  $\text{Ce}_{1-x}\text{Bi}_x\text{O}_{2-\delta}$  Solid Solution and Au/ $\text{Ce}_{1-x}\text{Bi}_x\text{O}_{2-\delta}$  for 5-Hydroxymethylfurfural Conversion in Alkaline Aqueous Solution. *Catal. Sci. Technol.* **2015**, *5*, 1314–1322. [\[CrossRef\]](#)
21. Ait Rass, H.; Essayem, N.; Besson, M. Selective Aerobic Oxidation of 5-HMF into 2,5-Furandicarboxylic Acid with Pt Catalysts Supported on  $\text{TiO}_2$ - and  $\text{ZrO}_2$ -Based Supports. *ChemSusChem* **2015**, *8*, 1206–1217. [\[CrossRef\]](#)
22. Ait Rass, H.; Essayem, N.; Besson, M. Selective Aqueous Phase Oxidation of 5-Hydroxymethylfurfural to 2,5-Furandicarboxylic Acid over Pt/C Catalysts: Influence of the Base and Effect of Bismuth Promotion. *Green Chem.* **2013**, *15*, 2240–2251. [\[CrossRef\]](#)
23. Siankevich, S.; Savoglidis, G.; Fei, Z.; Laurenczy, G.; Alexander, D.T.L.; Yan, N.; Dyson, P.J. A Novel Platinum Nanocatalyst for the Oxidation of 5-Hydroxymethylfurfural into 2,5-Furandicarboxylic Acid under Mild Conditions. *J. Catal.* **2014**, *315*, 67–74. [\[CrossRef\]](#)
24. Miao, Z.; Wu, T.; Li, J.; Yi, T.; Zhang, Y.; Yang, X. Aerobic Oxidation of 5-Hydroxymethylfurfural (HMF) Effectively Catalyzed by a  $\text{Ce}_{0.8}\text{Bi}_{0.2}\text{O}_{2-\delta}$  Supported Pt Catalyst at Room Temperature. *RSC Adv.* **2015**, *5*, 19823–19829. [\[CrossRef\]](#)
25. Davis, S.E.; Houk, L.R.; Tamargo, E.C.; Datye, A.K.; Davis, R.J. Oxidation of 5-Hydroxymethylfurfural over Supported Pt, Pd and Au Catalysts. *Catal. Today* **2011**, *160*, 55–60. [\[CrossRef\]](#)
26. Hu, L.; Zhao, G.; Hao, W.; Tang, X.; Sun, Y.; Lin, L.; Liu, S. Catalytic Conversion of Biomass-Derived Carbohydrates into Fuels and Chemicals via Furanic Aldehydes. *RSC Adv.* **2012**, *2*, 11184–11206. [\[CrossRef\]](#)
27. Rosatella, A.A.; Simeonov, S.P.; Frade, R.F.M.; Afonso, C.A.M. 5-Hydroxymethylfurfural (HMF) as a Building Block Platform: Biological Properties, Synthesis and Synthetic Applications. *Green Chem.* **2011**, *13*, 754–793. [\[CrossRef\]](#)
28. Xu, S.; Zhou, P.; Zhang, Z.; Yang, C.; Zhang, B.; Deng, K.; Bottle, S.; Zhu, H. Selective Oxidation of 5-Hydroxymethylfurfural to 2,5-Furandicarboxylic Acid Using  $\text{O}_2$  and a Photocatalyst of Co-Thioporphyrazine Bonded to  $\text{g-C}_3\text{N}_4$ . *J. Am. Chem. Soc.* **2017**, *139*, 14775–14782. [\[CrossRef\]](#)

29. Barwe, S.; Weidner, J.; Cychy, S.; Morales, D.M.; Dieckhöfer, S.; Hiltrop, D.; Masa, J.; Muhler, M.; Schuhmann, W. Electrocatalytic Oxidation of 5-(Hydroxymethyl)Furfural Using High-Surface-Area Nickel Boride. *Angew. Chem. Int. Ed.* **2018**, *57*, 11460–11464. [[CrossRef](#)]
30. Weidner, J.; Barwe, S.; Sliozberg, K.; Piontek, S.; Masa, J.; Apfel, U.P.; Schuhmann, W. Cobalt-Metalloid Alloys for Electrochemical Oxidation of 5-Hydroxymethylfurfural as an Alternative Anode Reaction in Lieu of Oxygen Evolution during Water Splitting. *Beilstein J. Org. Chem.* **2018**, *14*, 1436–1445. [[CrossRef](#)]
31. Lu, Y.; Dong, C.; Huang, Y.; Zou, Y.; Liu, Z.; Liu, Y.; Li, Y.; He, N.; Shi, J.; Wang, S. Identifying the Geometric Site Dependence of Spinel Oxides for the Electrooxidation of 5-Hydroxymethylfurfural. *Angew. Chem.* **2020**, *132*, 19377–19383. [[CrossRef](#)]
32. Chen, C.; Wang, L.; Zhu, B.; Zhou, Z.; El-Hout, S.I.; Yang, J.; Zhang, J. 2,5-Furandicarboxylic acid production via catalytic oxidation of 5-hydroxymethylfurfural: Catalysts, processes and reaction mechanism. *J. Energy Chem.* **2021**, *54*, 528–554. [[CrossRef](#)]
33. Deng, X.; Xu, G.; Zhang, Y.; Wang, L.; Zhang, J.; Li, J.; Fu, X.; Luo, J. Understanding the Roles of Electrogenerated  $\text{Co}^{3+}$  and  $\text{Co}^{4+}$  in Selectivity-Tuned 5-Hydroxymethylfurfural Oxidation. *Angew. Chem.* **2021**, *133*, 20698–20705. [[CrossRef](#)]
34. Ong, W.; Tan, L.; Ng, Y.H.; Yong, S.; Chai, S. Graphitic Carbon Nitride (g- $\text{C}_3\text{N}_4$ -Based Photocatalysts for Artificial Photosynthesis and Environmental Remediation: Are We a Step Closer to Achieving Sustainability? *Chem. Rev.* **2016**, *116*, 7159–7329. [[CrossRef](#)]
35. Suliman, M.A.; Suliman, M.H.; Adam, A.; Basheer, C.; Yamani, Z.H.; Qamar, M. Interfacial Coupling of Amorphous Cobalt Boride with G- $\text{C}_3\text{N}_4$  Nanosheets for Superior Oxygen Evolution Reaction. *Mater. Lett.* **2020**, *268*, 127593. [[CrossRef](#)]
36. Jiang, N.; You, B.; Boonstra, R.; Terrero Rodriguez, I.M.; Sun, Y. Integrating Electrocatalytic 5-Hydroxymethylfurfural Oxidation and Hydrogen Production via Co-P-Derived Electrocatalysts. *ACS Energy Lett.* **2016**, *1*, 386–390. [[CrossRef](#)]
37. Liu, S.; Tian, J.; Wang, L.; Zhang, Y.; Qin, X.; Luo, Y.; Asiri, A.M.; Al-youbi, A.O.; Sun, X. Hydrothermal Treatment of Grass: A Low-Cost, Green Route to Nitrogen-Doped, Carbon-Rich, Photoluminescent Polymer Nanodots as an Effective Fluorescent Sensing Platform for Label-Free Detection of Cu (II) Ions. *Adv. Mater.* **2012**, *24*, 2037–2041. [[CrossRef](#)]
38. Lei, W.; Portehault, D.; Dimova, R.; Antonietti, M. Boron Carbon Nitride Nanostructures from Salt Melts: Tunable Water-Soluble Phosphors. *J. Am. Chem. Soc.* **2011**, *133*, 7121–7127. [[CrossRef](#)]
39. Chen, Z.; Kang, Q.; Cao, G.; Xu, N.; Dai, H.; Wang, P. Study of Cobalt Boride-Derived Electrocatalysts for Overall Water Splitting. *Int. J. Hydrog. Energy* **2018**, *43*, 6076–6087. [[CrossRef](#)]
40. Dijkman, W.P.; Groothuis, D.E.; Fraaije, M.W. Enzyme-Catalyzed Oxidation of 5-Hydroxymethylfurfural to Furan-2,5-Dicarboxylic Acid. *Angew. Chem. Int. Ed.* **2014**, *53*, 6515–6518. [[CrossRef](#)]
41. Lv, G.; Wang, H.; Yang, Y.; Deng, T.; Chen, C.; Zhu, Y.; Hou, X. Graphene Oxide: A Convenient Metal-Free Carbocatalyst for Facilitating Aerobic Oxidation of 5-Hydroxymethylfurfural into 2,5-Diformylfuran. *ACS Catal.* **2015**, *5*, 5636–5646. [[CrossRef](#)]
42. Kang, M.J.; Park, H.; Jegal, J.; Hwang, S.Y.; Kang, Y.S.; Cha, H.G. Electrocatalysis of 5-Hydroxymethylfurfural at Cobalt Based Spinel Catalysts with Filamentous Nanoarchitecture in Alkaline Media. *Appl. Catal. B Environ.* **2019**, *242*, 85–91. [[CrossRef](#)]
43. Zhang, M.; Liu, Y.; Liu, B.; Chen, Z.; Xu, H.; Yan, K. Trimetallic NiCoFe-Layered Double Hydroxides Nanosheets Efficient for Oxygen Evolution and Highly Selective Oxidation of Biomass-Derived 5-Hydroxymethylfurfural. *ACS Catal.* **2020**, *10*, 5179–5189. [[CrossRef](#)]
44. Cai, M.; Zhang, Y.; Zhao, Y.; Liu, Q.; Li, Y.; Li, G. Two-Dimensional Metal-Organic Framework Nanosheets for Highly Efficient Electrocatalytic Biomass 5-(Hydroxymethyl)Furfural (HMF) Valorization. *J. Mater. Chem. A* **2020**, *8*, 20386–20392. [[CrossRef](#)]
45. Zhang, N.; Zou, Y.; Tao, L.; Chen, W.; Zhou, L.; Liu, Z.; Zhou, B.; Huang, G.; Lin, H.; Wang, S. Electrochemical Oxidation of 5-Hydroxymethylfurfural on Nickel Nitride/Carbon Nanosheets: Reaction Pathway Determined by In Situ Sum Frequency Generation Vibrational Spectroscopy. *Angew. Chem.* **2019**, *131*, 16042–16050. [[CrossRef](#)]
46. You, B.; Jiang, N.; Liu, X.; Sun, Y. Simultaneous  $\text{H}_2$  Generation and Biomass Upgrading in Water by an Efficient Noble-Metal-Free Bifunctional Electrocatalyst. *Angew. Chem.* **2016**, *128*, 10067–10071. [[CrossRef](#)]
47. Taitt, B.J.; Nam, D.H.; Choi, K.S. A Comparative Study of Nickel, Cobalt, and Iron Oxyhydroxide Anodes for the Electrochemical Oxidation of 5-Hydroxymethylfurfural to 2,5-Furandicarboxylic Acid. *ACS Catal.* **2019**, *9*, 660–670. [[CrossRef](#)]
48. Cardiel, A.C.; Taitt, B.J.; Choi, K.S. Stabilities, Regeneration Pathways, and Electrocatalytic Properties of Nitroxyl Radicals for the Electrochemical Oxidation of 5-Hydroxymethylfurfural. *ACS Sustain. Chem. Eng.* **2019**, *7*, 11138–11149.
49. Qian, G.; Yu, G.; Lu, J.; Luo, L.; Wang, T.; Zhang, C.; Ku, R.; Yin, S.; Chen, W.; Mu, S. Ultra-thin N-doped-graphene encapsulated Ni nanoparticles coupled with  $\text{MoO}_2$  nanosheets for highly efficient water splitting at large current density. *J. Mater. Chem. A* **2020**, *8*, 14545–14554. [[CrossRef](#)]
50. Wang, L.; Cao, J.; Lei, C.; Dai, Q.; Yang, B.; Li, Z.; Zhang, X.; Yuan, C.; Lei, L.; Hou, Y. Strongly coupled 3D N-doped  $\text{MoO}_2/\text{Ni}_3\text{S}_2$  hybrid for high current density hydrogen evolution electrocatalysis and biomass upgrading. *ACS Appl. Mater. Interfaces* **2019**, *11*, 27743–27750. [[CrossRef](#)]